# A Fully Coplanar D-A Polymeric Semiconductor with Promoted Charge Separation Kinetics for Photochemistry

Zhi-An Lan,[a, b] Meng Wu,[a] Zhongpu Fang,[a] Xu Chi,[a] Xiong Chen,*[a] Yongfan Zhang,[a] and Xinchen Wang*[a]

[a] Dr. Z. A. Lan, M. Wu, Z. Fang, X. Chi, Prof. X. Chen, Prof. Y. Zhang, Prof. X. Wang
State Key Laboratory of Photocatalysis on Energy and Environment, College of Chemistry
Fuzhou University
Fuzhou 350116 (P.R. China)
E-mail: chenxiong987@fzu.edu.cn; xcwang@fzu.edu.cn
Homepage: http://wanglab.fzu.edu.cn

[b] Dr. Z. A. Lan
College of Chemical Engineering
Fuzhou University
Fuzhou 350116 (P. R. China)

Supporting information for this article is given via a link at the end of the document.

**Abstract:** Charge generation and separation are regarded as the major constraints limiting the photocatalytic activity of polymeric photocatalysts. Herein, two new linear polyarylether-based polymers (PAE-CPs) with distinct linking patterns between their donor and acceptor motifs were tailor-made to investigate the influence of different linking patterns on the charge generation and separation process. Theoretical and experimental results revealed that compared to the traditional single-stranded linker, the double-stranded linking pattern strengthens donor-acceptor interactions in PAE-CPs and generates a coplanar structure, facilitating charge generation and separation, and enabling red-shifted light absorption. With these prominent advantages, the PAE-CP interlinked with a double-stranded linker exhibits markedly enhanced photocatalytic activity compared to that of its single-strand-linked analogue. Such findings can facilitate the rational design and modification of organic semiconductors for charge-induced reactions.

Converting solar energy into chemical energy via photocatalysis is an attractive energy utilization technique for a sustainable future.[1] Conjugated polymers (CPs) have recently emerged as promising photocatalysts, as their frameworks and properties are amenable to modification via topological molecular engineering.[2] Thus far, numerous conjugated polymer photocatalysts with various molecular structures have been developed, such as carbon nitride, linear polymers, conjugated porous polymers (CPPs), conjugated triazine-based polymers (CTPs), and covalent organic frameworks (COFs).[3] Nevertheless, for the majority of polymer photocatalysts, the charge generation and separation process is far from satisfactory, especially when compared with the efficiency of inorganic materials.[4]

The most common and efficient strategy for promoting the charge generation and separation process in polymer photocatalysts is to construct a donor-acceptor (D-A) system.[5] Due to the presence of a polarized electric field, photogenerated charges in a D-A polymer can be rapidly separated via intramolecular charge transfer (ICT). Based on this strategy, diverse donor and acceptor building blocks have been designed to establish D-A type polymers and achieve considerable photocatalytic activity, such as the commonly used sulfone-containing units and aromatic nitriles.[6] Recent advancements have revealed that donor or acceptor units with planar structures are favored as they reduce the exciton binding energy and enhance the charge mobility of the corresponding D-A polymer.[7] However, in the majority of the reported D-A polymer photocatalysts, the donor and acceptor motifs are connected by a single-stranded linker, which often results in a non-planar arrangement between them (Scheme 1a, left). In this case, finding a suitable strategy to minimize this torsion and build a fully coplanar polymer skeleton is highly desired to improve charge generation and separation in the D-A polymer, and in turn achieve efficient photocatalytic performances.

Polyarylether (PAE), generated by linking various aromatic rings with ether bonds, is a widely used polymeric material in the plastics engineering industry.[8] Numerous studies have implied that the excellent thermal and chemical stability of PAEs may also satisfy the requirements for photocatalytic applications.[9] More importantly, we can introduce double ether bonds between their donor and acceptor motifs by generating a benzodioxane moiety (Scheme 1b)[10] to afford polyarylether-based conjugated polymers (PAE-CPs) with a double-stranded linking pattern. This unique linking pattern would be beneficial for suppressing the free rotation of the linking bond and theoretically lead to a fully coplanar polymer skeleton (Scheme 1a, right). Therefore, PAE-CPs have the potential to deliver fully coplanar D-A polymer photocatalysts. Furthermore, they could be ideal candidates for investigating differences in the effects of single- and double-stranded linkers on the photocatalytic performance of D-A polymers, and therefore contribute to advancements in this field.

Herein, we performed a proof-of-concept study on the linking patterns of PAE-CPs and explored their influence on the charge generation and separation processes. The two PAE-CPs depicted in Scheme 1c comprise benzene rings as the donors and terephthalonitrile units as the acceptors, linked by ether bonds. However, the linking pattern in the two PAE-CPs is different. The donor and acceptor in PAE-S are connected by a single ether bond to generate a single-stranded linking pattern; in contrast, PAE-D contains two ether bonds between a set of donor and acceptor motifs, creating a double-stranded linking pattern. A combination of experimental and theoretical studies of these PAE-CPs would provide crucial information for the design and modulation of linking patterns for promoting charge

generation and separation in D-A conjugated polymer photocatalysts, to achieve efficient photocatalytic performance.

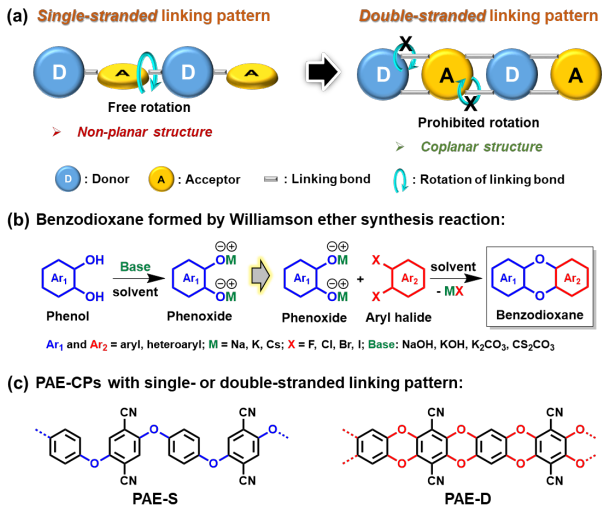


**Scheme 1.** a) Graphical representation of two types of D-A polymers with different linking patterns. b) Synthetic route to benzodioxane. c) Molecular structures of the two PAE-CPs used in this study.

To prepare the targeted PAE-CPs, a typical Williamson ether synthesis reaction was performed between the corresponding hydroxybenzene and terephthalonitrile halide (see experimental details in the Supporting Information). Both PAE-CPs were insoluble solids with a semi-crystalline structure, as inferred from their powder X-ray diffraction patterns (PXRD, Figure S1). Their scanning electron microscopy (SEM, Figure S2 and S3) images show that both the PAE-CPs exhibited nanoparticle-like morphology, and no obvious pores were observed, owing to the low-porosity of the linear polymer. Therefore, both PAE-CPs present low apparent Brunauer-Emmett-Teller (BET) surface areas (approximately 10 $m^2 g^{-1}$), as calculated from the nitrogen adsorption isotherms measured at 77 K (Figure S3 and S4, Table 1). The low-porosity nanoparticle-like morphologies of the PAE-CPs were also clearly observed in their transmission electron microscopy (TEM) images (Figure 1a and S6). Additionally, elemental mapping of both PAE-CPs indicated that the major elements (C, N, and O) were uniformly distributed throughout the entire selected area.

**Table 1.** Physicochemical properties of the as-prepared PAE-CPs.

| Polyarylether | $S_{BET}$[a] [$m^2 g^{-1}$] | DA[b] [°] | $Ave_{Charges}$-D[c] [e] | OG[d] [eV] | $E_a$[e] [meV] |
|---|---|---|---|---|---|
| PAE-S | 10 | 90.0 | 1.20 | 3.05 | 60 |
| PAE-D | 8 | 0.0 | 2.19 | 2.32 | 42 |

[a] Specific surface areas were derived from $N_2$ adsorption isotherms. [b] Dihedral angle (DA) between neighbor donor and acceptor was obtained from DFT calculations. [c] The average of the Bader charges of donor moieties (benzene rings) in each PAE-CP was acquired by calculation, and a positive value implies loss of electrons. [d] The optical gap (OG) was estimated from the absorption edge. [e] Activation energy of the photoluminescence quenching process deduced from temperature-dependent photoluminescence spectra.

To further confirm the successful preparation of the targeted PAE-CPs, a series of chemical structure analyses, including elemental analysis (Table S1), Fourier transform infrared (FT-IR) spectroscopy (Figure S7 and S8), X-ray photoelectron spectroscopy (XPS, Figure 1b and S9-12), and solid-state $^{13}C$ nuclear magnetic resonance ($^{13}C$ ssNMR) spectroscopy (Figure 1c), were subsequently conducted. As shown in the FT-IR spectra of both PAE-CPs, the vibration signal present at approximately 2252 $cm^{-1}$ arises from the cyano group.[11] The two absorption peaks at 1271 $cm^{-1}$ and 1010 $cm^{-1}$ for PAE-S and at 1257 $cm^{-1}$ and 1010 $cm^{-1}$ for PAE-D originate from the symmetric and asymmetric vibrational modes of the ether bonds, respectively.[9a] Notably, the relative intensity of these two peaks is significantly stronger for PAE-D than in PAE-S, suggesting the presence of a higher number of ether bonds in PAE-D. These structural features were further verified by XPS spectroscopy. As displayed in Figure 1b, the C 1s XPS spectra of both PAE-CPs can be resolved into three major peaks, assigned to the $sp^2$-hybrid C species in the aromatic ring (C1), sp-hybrid C species in the cyano group (C2), and the C species of the ether bond.[12] The experimental ratios of each C species for both PAE-CPs were in agreement with the calculated values (Table S2), and due to the additional ether bonds in the molecular structure of PAE-D, the ratio of C3 species (C-O) in PAE-D is significantly higher than in PAE-S (Table S2). This result is consistent with the results of FT-IR analysis. Furthermore, all the distinct C species in the molecular structure of PAE-S or PAE-D were unambiguously identified by the corresponding peaks in the $^{13}C$ ssNMR spectra, further confirming the formation of the targeted PAE-CPs (Figure 1c).

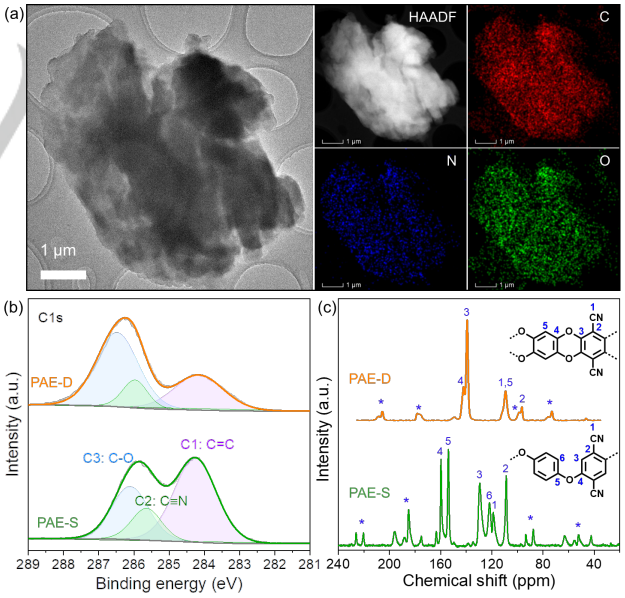


**Figure 1.** a) TEM image of PAE-S with elemental maps for C, N, and O. b) C 1s XPS spectra of the PAE-CPs. c) Solid-state $^{13}C$ NMR spectra of the PAE-CPs.

To investigate the structural features of the linking patterns in the PAE-CPs, density functional theory (DFT) calculations were conducted for PAE-S and PAE-D monolayers, simulated by periodic structures (see Supporting Information for details). As

portrayed in Figure 2a, the optimized geometric configuration of PAE-S presents a distorted linear structure, and the dihedral angle between neighboring aromatic rings is as large as 90.0°. This highly distorted geometry likely reduces conjugation within the polymer and prohibits charge transfer through the polymeric backbone, which is detrimental to photocatalysis efficiency. As expected, the introduction of an additional ether bond into the molecular structure yields a double-stranded linking pattern, which results in a coplanar structure, and the dihedral angle between neighboring aromatic rings becomes 0.0°. Hence, we can confirm that the double-stranded linking pattern allows for the construction of a coplanar structure, which in principle, promotes charge-separation efficiency. In addition, by calculating the Bader charge of every atom in the unit cell of PAE-S and PAE-D (Figure S13), it was found that the average of the donor fragment Bader charges ($Ave_{Charges}$-D) was considerably higher in PAE-D than in PAE-S (Table 1), indicating that the acceptor motifs in PAE-D had enhanced electron-withdrawing properties. Hence, we can infer that the additional ether bonds in PAE-D can markedly strengthen D-A interactions in the polymer structure and reduce the band gap energy, and thereby affect the charge generation process during photocatalysis.

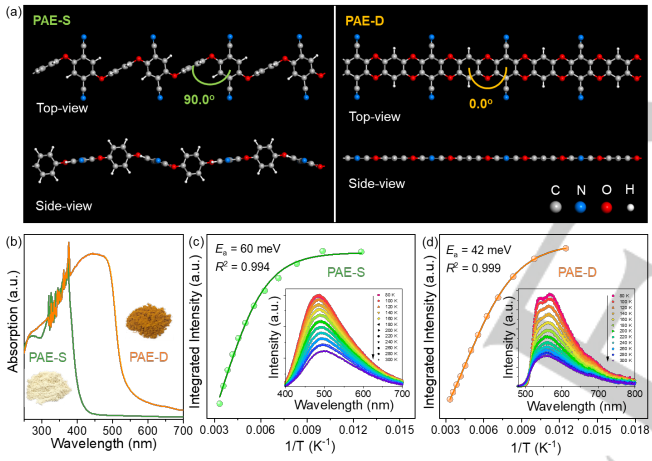


**Figure 2.** a) DFT geometry optimization of PAE-S and PAE-D monolayers simulated using a periodic structure. b) UV-Vis DRS of PAE-CPs. c) and d) Integrated PL emission intensity as a function of temperature from 80 to 300 K (Inset: temperature-dependent PL spectra) of the PAE-CPs.

To further experimentally investigate the effect of different PAE-CP linking patterns on the charge generation and separation process, we conducted a series of optical and electrochemical measurements. First, the light harvesting ability of the PAE-CPs was assessed by UV-Vis diffuse reflectance spectroscopy (UV-Vis DRS). As shown in Figure 2b, the two polymers both display typical optical absorption behavior induced by π-π* electron transitions in the conjugated aromatic scaffold. The absorption edge of PAE-S was determined to be 406 nm, which corresponds to an optical gap of 3.05 eV. Additionally, a slight absorption tail terminating at approximately 460 nm was also detected. However, for PAE-D, the intrinsic optical absorption range is significantly extended to 535 nm, promoting the utilization of visible photons for inducing free charges. In view of these calculation outcomes, we can conclude that this increased optical absorption behavior of PAE-D arises from the extended conjugation and stronger D-A interactions resulting from its double-stranded linking pattern.

Furthermore, temperature-dependent photoluminescence (PL) spectra of the PAE-CPs were obtained to elucidate their charge recombination and separation kinetics. As shown in the temperature-dependent PL spectra (Figure 2c inset and 2d inset), both polymers exhibited the thermal quenching phenomenon of PL emission in the temperature range from 80 to 300 K. By fitting the integrated PL intensities as a function of temperature using the Arrhenius equation: $I(T) = I_0/(1 + A \exp(-E_a/k_BT))$, we can obtain the activation energy ($E_a$) of the PL quenching process.[13] Accordingly, as shown in Figure 2c and 2d, the $E_a$ for PAE-S and PAE-D was estimated to be 60 and 42 meV, respectively. The lower $E_a$ value for PAE-D implies that non-radiative pathways, such as charge separation (in some cases, equal to exciton splitting), would occur more readily in PAE-D.[14] Indeed, in a direct comparison of room-temperature PL intensities of the two PAE-CPs (Figure S14), it is evident that PAE-D manifests a significantly lower PL intensity than PAE-S. Thus, we can surmise that the double-stranded linking pattern is advantageous for promoting charge separation in D-A polymer photocatalysts.

Moreover, photoelectrochemical measurements offered further significant evidence. As shown in Figure S17 and S18, owing to its planar conformation, PAE-D consistently presented smaller radii of its semi-circular Nyquist plots than PAE-S in electrochemical impedance spectroscopy (EIS) measurements in the presence or absence of light irradiation, suggesting lower charge transfer resistance in PAE-D. Similarly, PAE-D also displayed a higher photocurrent response in photocurrent measurements (Figure S19). These results are consistent with the conclusions drawn from PL analyses.

The photocatalytic activity of the PAE-CPs was first evaluated by analyzing the hydrogen evolution reaction (HER) under light irradiation. These tests were conducted with 3 wt.% (theoretical amount) photodeposited Pt as the cocatalyst (Figure S23 and S24; the actual loading contents of Pt on PAE-S and PAE-D determined by ICP-MS measurements were 1.0% and 1.1%, respectively). As displayed in Figure 3a, PAE-S achieves a HER rate of 130 μmol $h^{-1}$ upon broadband light irradiation (λ ≥ 300 nm). However, when light irradiation was narrowed to the visible region (λ ≥ 420 nm), the HER rate declined sharply to 24 μmol $h^{-1}$. In contrast, PAE-D maintained a high HER rate (120 μmol $h^{-1}$) even under visible-light irradiation, and achieved an apparent quantum yield (AQY) of 5.6% (λ = 420 nm), which was considerably higher than that of PAE-S ($AQY_{420nm}$ = 0.8%). Moreover, even in the absence of the Pt cocatalyst, PAE-D still presented a higher HER of the two PAE-CPs (Figure S25). This remarkable photocatalytic performance of PAE-D arises from the optimized charge generation and separation, enabled by the double-stranded linking pattern and increased planarity of the geometric construction. Moreover, the HER activity of PAE-D (Figure 3b) remained high during the 5-circles test (20 h), suggesting that PAE-D is a stable photocatalyst.

In addition, the photocatalytic performance of the PAE-CPs was evaluated by a second assay entailing $H_2O_2$ production via oxygen reduction. As shown in Figure 3c, both PAE-CPs exhibited photoactivity toward $H_2O_2$ production. It is noteworthy that only a few polymer photocatalysts have been reported to mediate this reaction thus far.[15] Similar to the $H_2$ evolution

reaction, the $H_2O_2$ evolution reaction (HPER) rate of PAE-D was more than double that of PAE-S. To investigate the $H_2O_2$ production pathway during photocatalysis, we further performed the test in different atmospheres. As illustrated in Figure 3d, the HPER rate for PAE-D was highest in pure $O_2$, significantly lower in air, and nearly completely inhibited in Ar. This strongly suggests that $H_2O_2$ was produced via oxygen reduction.

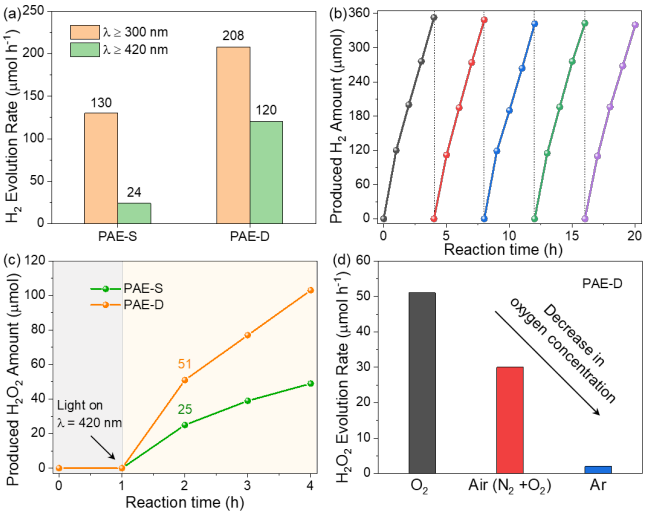


**Figure 3.** Photocatalytic performances of the PAE-CPs. a) $H_2$ evolution rates; Reaction conditions: 50 mg PAE-CP, 3 wt.% Pt cocatalyst (theoretical amount), 10 mL TEOA, 100 mL $H_2O$, 300 W Xe lamp with cut-off filter λ > 300 or 420 nm. b) Long-term $H_2$ evolution by PAE-D under visible-light irradiation (λ ≥ 420 nm). c) Time dependence of $H_2O_2$ evolution; Reaction conditions: 20 mg PAE-CP, 2 mL isopropanol, 18 mL $H_2O$, 1 atm $O_2$, 298 K, 420 nm monochromatic LED lamp. d) Influence of $O_2$ concentration on the $H_2O_2$ evolution rate of the PAE-D photocatalyst.

In summary, we have designed two new linear PAE-CPs with single/ double-stranded linkers between their donor and acceptor motifs to explore the influence of the two linking patterns on the charge generation and separation processes. By combining theoretical and experimental studies, we have established that the double-stranded linking pattern is beneficial for strengthening D-A interactions in the PAE-CP and for constructing a coplanar structure, which in turn promotes charge generation and separation and enhances optical absorption. Thus, PAE-D with a double-stranded linking pattern exhibits a superior photocatalytic performance to that of PAE-S, containing a single-stranded linker, upon visible-light irradiation. Notably, this is the first attempt to utilize PAE-CPs for artificial photosynthesis of hydrogen and hydrogen peroxide. The findings of this study can contribute to the advancement of D-A conjugated polymer photocatalyst designs for future artificial photosynthetic applications.

## Acknowledgements

This work was financially supported by the National Natural Science Foundation of China (22032002, 21972021, U1905214, 21961142019, 21861130353, 21425309, 21761132002, and 22002017), the National Basic Research Program of China (2013CB632405), the Chang Jiang Scholars Program of China (T2016147), the National Postdoctoral Program for Innovative Talents (BX20200084), and the 111 Project (D16008).

**Keywords:** photocatalysis • polyarylether • linking pattern • hydrogen evolution • hydrogen peroxide evolution

[1] a) Q. Wang, K. Domen, *Chem. Rev.* **2019**, *120*, 919-985; b) Y. Fang, Y. Zheng, T. Fang, Y. Chen, Y. Zhu, Q. Liang, H. Sheng, Z. Li, C. Chen, X. Wang, *Sci. China Chem.* **2020**, *63*, 149-181.

[2] a) G. Zhang, Z. A. Lan, X. Wang, *Angew. Chem. Int. Ed.* **2016**, *55*, 15712-15727; b) X. Chen, K. Geng, R. Liu, K. T. Tan, Y. Gong, Z. Li, S. Tao, Q. Jiang, D. Jiang, *Angew. Chem. Int. Ed.* **2020**, *59*, 5050-5091; c) M. Ismael, Y. Wu, *Sustain. Energy Fuels* **2019**, *3*, 2907-2925; d) X. Huang, C. Sun, X. Feng, *Sci. China Chem.* **2020**, *63*, 1367-1390.

[3] a) X. Wang, K. Maeda, A. Thomas, K. Takanabe, G. Xin, J. M. Carlsson, K. Domen, M. Antonietti, *Nat. Mater.* **2009**, *8*, 76-80; b) L. H. Lin, Z. Y. Lin, J. Zhang, X. Cai, W. Lin, Z. Y. Yu, X. C. Wang, *Nat. Catal.* **2020**, *3*, 649-655; c) M. Liu, Q. Huang, S. Wang, Z. Li, B. Li, S. Jin, B. Tan, *Angew. Chem. Int. Ed.* **2018**, *57*, 11968-11972; d) X. Wang, L. Chen, S. Y. Chong, M. A. Little, Y. Wu, W. H. Zhu, R. Clowes, Y. Yan, M. A. Zwijnenburg, R. S. Sprick, A. I. Cooper, *Nat. Chem.* **2018**, *10*, 1180-1189; e) E. Jin, Z. Lan, Q. Jiang, K. Geng, G. Li, X. Wang, D. Jiang, *Chem* **2019**, *5*, 1632-1647; f) W. H. Wang, L. Y. Ting, J. Jayakumar, C. L. Chang, W. C. Lin, C. C. Chung, M. H. Elsayed, C. Y. Lu, A. M. Elewa, H. H. Chou, *Sustain. Energy Fuels* **2020**, *4*, 5264-5270.

[4] a) H. Wang, S. Jin, X. Zhang, Y. Xie, *Angew. Chem. Int. Ed.* **2020**, *59*, 22828-22839; b) Z.-A. Lan, W. Ren, X. Chen, Y. Zhang, X. Wang, *Appl. Catal. B* **2019**, *245*, 596-603; c) Y. Zheng, Y. L. Chen, L. Wang, M. Y. Tan, Y. Y. Xiao, B. F. Gao, B. Z. Lin, *Sustain. Energy Fuels* **2020**, *4*, 3739-3746.

[5] a) C. Yang, B. C. Ma, L. Zhang, S. Lin, S. Ghasimi, K. Landfester, K. A. Zhang, X. Wang, *Angew. Chem. Int. Ed.* **2016**, *55*, 9202-9206; b) Z.-A. Lan, Y. Fang, Y. Zhang, X. Wang, *Angew. Chem. Int. Ed.* **2018**, *57*, 470-474.

[6] a) Y. Bai, L. Wilbraham, B. J. Slater, M. A. Zwijnenburg, R. S. Sprick, A. I. Cooper, *J. Am. Chem. Soc.* **2019**, *141*, 9063-9071; c) J. Xu, C. Yang, S. Bi, W. Wang, Y. He, D. Wu, Q. Liang, X. Wang, F. Zhang, *Angew. Chem. Int. Ed.* **2020**, *59*, 23845-23853.

[7] a) Z. A. Lan, G. Zhang, X. Chen, Y. Zhang, K. A. I. Zhang, X. Wang, *Angew. Chem. Int. Ed.* **2019**, *58*, 10236-10240; b) Z. J. Wang, X. Y. Yang, T. J. Yang, Y. B. Zhao, F. Wang, Y. Chen, J. H. Zeng, C. Yan, F. Huang, J. X. Jiang, *ACS Catal.* **2018**, *8*, 8590-8596.

[8] P. M. Hergenrother, *High Perform. Polym.* **2003**, *15*, 3-45.

[9] a) X. Guan, H. Li, Y. Ma, M. Xue, Q. Fang, Y. Yan, V. Valtchev, S. Qiu, *Nat. Chem.* **2019**, *11*, 587-594; b) N. B. McKeown, P. M. Budd, *Chem. Soc. Rev.* **2006**, *35*, 675-683.

[10] N. B. McKeown, B. Gahnem, K. J. Msayib, P. M. Budd, C. E. Tattershall, K. Mahmood, S. Tan, D. Book, H. W. Langmi, A. Walton, *Angew. Chem. Int. Ed.* **2006**, *45*, 1804-1807.

[11] Z. A. Lan, Y. Fang, X. Chen, X. Wang, *Chem. Commun.* **2019**, *55*, 7756-7759.

[12] a) D. Briggs, G. Beamson, *Analytical Chemistry* **1992**, *64*, 1729-1736; b) L. J. Matienzo, *Polymer* **1991**, *32*, 3057-3061.

[13] P. Misra, T. K. Sharma, L. M. Kukreja, *Curr. Appl. Phys.* **2009**, *9*, 179-183.

[14] a) Z. Chen, C. L. Yu, K. Shum, J. J. Wang, W. Pfenninger, N. Vockic, J. Midgley, J. T. Kenney, *J. Lumines.* **2012**, *132*, 345-349; b) J. Li, X. Yuan, P. Jing, J. Li, M. Wei, J. Hua, J. Zhao, L. Tian, *RSC Adv.* **2016**, *6*, 78311-78316.

[15] a) H. Ou, P. Yang, L. Lin, M. Anpo, X. Wang, *Angew. Chem. Int. Ed.* **2017**, 56, 10905-10910; b) C. Krishnaraj, H. Sekhar Jena, L. Bourda, A. Laemont, P. Pachfule, J. Roeser, C. V. Chandran, S. Borgmans, S. M. J. Rogge, K. Leus, C. V. Stevens, J. A. Martens, V. Van Speybroeck, E. Breynaert, A. Thomas, P. Van Der Voort, *J. Am. Chem. Soc.* **2020**, 142, 20107-20116.

## Entry for the Table of Contents

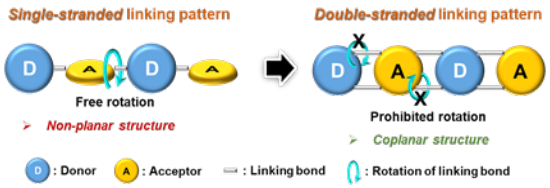


Two polyarylether-based polymers with single/ double linking patterns were investigated to establish the effect of the linking patterns on the charge generation and separation process in D-A conjugated polymer photocatalysts, thus achieving remarkable photocatalytic HER and HPER performances.